JOURNAL OF MATERIALS SCIENCE 20 (1985) 1049–1060

Residual strength of ground hot isostatically pressed silicon nitride

M. HAKULINEN*
Development and Production Section, Material and Strength Laboratory, Saab-Scania AB, Scania Division, S-151 87 Södertälje, Sweden

Surface flaws are introduced during grinding of most high strength ceramics. These flaws reduce the strength and it is therefore important to choose grinding parameters such that surface damage is minimized. The assumption that it is the same mechanism that causes cracking beneath both an indenter and a diamond tool made it possible to propose a grinding model. According to this model high wheel speeds, low workpiece velocities and low depths of cut would reduce the grinding forces and thus be beneficial to the strength after grinding. Grinding experiments on hot isostatically pressed silicon nitride showed that this was the case. The experiments also showed that the grinding direction had the strongest influence on the strength, and if possible the direction ought to be parallel with the expected principal stress. Even what can be considered to be mild machine parameters introduce flaws and residual compressive stresses in the surface of the workpiece.

1. Introduction

High strength ceramics (alumina, silicon nitride, silicon carbide, zirconia and others) are candidate materials for use in future combustion engines [1–4]. Engine components usually have rather close tolerances, and it will probably not be possible to sinter such ceramic parts to their final shape. This means that they will have to be machined after sintering.

The most common method of machining these materials is grinding with a diamond tool. From the material's point of view this must be a very rough method, since the diamonds are forced into the surface. It is therefore no surprise that the grinding operation causes decreased mechanical strength of the machined components, which has frequently been reported in the literature [5–25]. This reduction in strength is caused by cracks introduced into the surface layer during machining [7–16, 21, 23–25]. It has been shown that cracks perpendicular to the grinding direction are half-penny-shaped [9, 12, 16, 21, 24], whilst those parallel to the grinding direction more or less continuously follow the grinding groove [9, 12, 16, 21, 23, 24]. The latter cracks seem to be deeper than the former [9, 12, 16] and they probably consist of halfpenny-shaped defects so close together that they in fact form an elongated crack [24].

Since grinding with diamond tools seems to cause defects similar to those found beneath an indent [12, 24, 26] or a scratch [8, 23] made by a Vicker's diamond, indentation [12, 24] and scratching [8, 23] methods have been used to illustrate the mechanisms involved during grinding.

The aim of this work is to present a model in which it is assumed that grinding defects are of the same kind as those caused by a Vicker's indenter. If in fact this is the case it is possible to combine the equations valid for indentation [8, 24, 26, 27] and grinding [11, 28], respectively. With the resulting expression one ought to be able to illustrate how the strength after a grinding operation will depend on the machining parameters and the material properties of the workpiece.

*Present address: Uddeholm Strip Steel AB, PO Box 503, S-684 01 Munkfors, Sweden.

0022–2461/85 $03.00 + .12

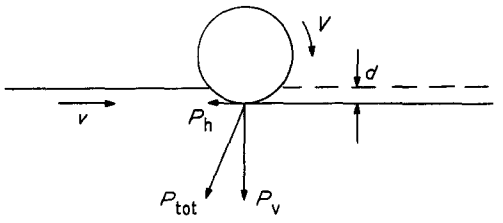

Figure 1 Definition of machine parameters and grinding forces occurring during grinding.

2. Model

2.1. Grinding forces

During the machining of the workpiece grinding forces arise. The magnitude of these forces depends on the machine parameters and the properties of the workpiece. In Fig. 1 the horizontal (P_h), vertical (P_v) and total (P_{tot}) forces are defined together with machine parameters as depth of cut (d), grinding wheel speed (V) and workpiece velocity (v). The horizontal and the vertical forces are related to each other through the expression [28]:

$$\frac{P_v}{P_h} = C, \tag{1}$$

where C is a variable which is a function of the machine parameters and the material properties of the workpiece.

The horizontal force depends on the machine parameters according to

$$P_h = u\left(\frac{vd}{V}\right)w \tag{2}$$

where w is the width on which the grinding wheel operates and u is the specific grinding energy [11, 28]. The latter depends on the machine parameters according to

$$u = u_0\left(\frac{vd}{V}\right)^a \tag{3}$$

where u_0 and a are material dependent factors [29].

Other parameters influencing the grinding forces, probably through the factors u_0 and a, are down or up grinding [30], the construction and condition of the diamond wheel [5–9, 11, 18, 25, 31–37] and if wet or dry grinding is used [31–33].

If one assumes that the variable C, in Equation 1, shows a similar dependence to u, in Equation 3, one obtains

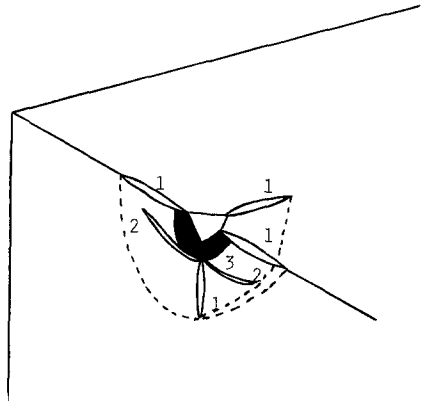

Figure 2 Fracture surface of a bend test bar, indented prior to the bend test. 1. Radial cracks; 2. lateral cracks; 3. plastic zone.

$$C = C_0\left(\frac{vd}{V}\right)^b, \tag{4}$$

where C_0 and b are related to the machining conditions. A combination of Equations 1 to 4 gives

$$P_v = u_0 C_0\left(\frac{vd}{V}\right)^{1+a+b} w. \tag{5}$$

During grinding frictional forces are generated in the area where the diamond wheel and the workpiece are in contact. In the following equation,

$$P_v = P_{0v} + u_0 C_0\left(\frac{vd}{V}\right)^{1+a+b} w, \tag{6}$$

P_{0v} is the vertical component of the frictional force occurring when the depth of cut is set to zero. P_{0v} is influenced by the properties of the grinding wheel and the workpiece material.

2.2. Surface cracks caused by a Vicker's indenter

In Fig. 2 the fracture surface of a broken bend test bar is sketched. Prior to the bend testing the bar was indented with a Vicker's indenter. Two kinds of cracks originate from the indent – lateral and radial cracks. The latter are halfpenny-shaped and are located along the indent diagonals, while the former are parallel to the bar surface [12, 15, 24, 26, 27].

The fracture strength of the bar is controlled by the size of the radial cracks, which are perpendicular to the bending direction. The size of these

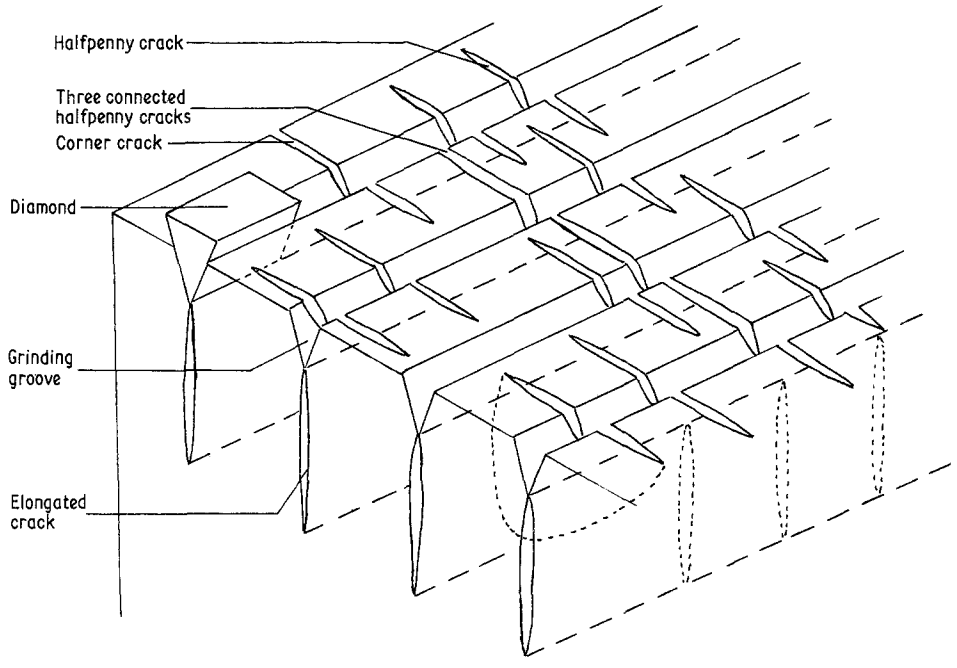

Figure 3 Elongated and halfpenny-shaped surface cracks caused by grinding with a diamond tool.

cracks strongly depends on the indenter load (P) and the residual strength of the bar, σ, can be estimated using Equation 7:

$$\sigma = \sigma_0 + A\left(\frac{H}{E}\right)^{1/6} K_{IC}^{4/3} \frac{1}{P^{1/3}} \quad (7)$$

where H is the Vicker's hardness, E the Young's modulus [24, 27], and K_{IC} the fracture toughness of the workpiece material. The term σ_0 has been added to compensate for residual surface stresses, existing prior to indentation. The residual stresses which are caused by the indenter have been considered during the derivation of Equation 7. According to the equation below,

$$A = [\tfrac{256}{27}(\pi 1.25 f^2)^{3/2} B (\cot \Psi)^{2/3}]^{-1/3}, \quad (8)$$

A is a variable which depends on the geometry of the indenter, the indented component and the resulting crack. In Equation 8 2Ψ is the angle between opposite edges of the indenter, B a dimensionless factor dependent on the indenter geometry [24, 26, 27, 38] and f a geometric factor.

2.3. Surface defects introduced by grinding

According to the literature references in Section 1 the cracks parallel to the grinding direction are more elongated and deeper than those perpendicular to the grinding direction. These two kinds of crack systems are illustrated schematically in Fig. 3. No explanation as to why the depth of the cracks depends on the grinding direction has been found in the literature. However, it is reasonable to assume that the elongated cracks are caused by higher grinding forces than the halfpenny-shaped ones. From Fig. 1 one can assume that it is the total grinding force P_{tot} that has caused the former cracks and the vertical grinding force P_v the latter. This means that the total grinding force can be expressed as:

$$P_{tot} = P_v\left(1 + \frac{P_h}{P_v}\sin\Theta\right) \quad (9)$$

where Θ is 90° and 0° for transverse and longitudinal grinding, respectively.

The difference in the geometry and the depth of the cracks naturally makes the residual strength dependent on the grinding direction. In the literature it has been reported that transverse grinding, compared to longitudinal, can reduce the residual strength by as much as 50% [5, 6, 9, 10, 12, 13, 15–17, 20, 21, 25]. With the Equations 10 and 11

$$\sigma = \frac{K_{IC}}{1.12 f (\pi c)^{1/2}} \quad (10)$$

$$f = 1 - 0.37 \cos\Theta \quad (11)$$

TABLE I The expected influence of some grinding parameters on the total grinding force and the residual strength, according to the Equations 6, 9 and 13

Parameter	Factor influenced	Effect on:	
		P_{tot}	σ
Wheel speed	$\uparrow V$	$\downarrow$	$\uparrow$
Workpiece velocity	$\uparrow v$	$\uparrow$	$\downarrow$
Depth of cut	$\uparrow d$	$\uparrow$	$\downarrow$
Longitudinal grinding	$\downarrow f$	$\downarrow$	$\uparrow$
Transverse grinding	$\uparrow f$	$\uparrow$	$\downarrow$

TABLE III Machine parameters used in this investigation

Wheel speed ($m\,sec^{-1}$)	Workpiece velocity ($m\,min^{-1}$)	Depth of cut (mm)
10	10	0.01/0.03
20	10	0.01/0.03
30	10	0.01/0.03
10	20	0.01/0.03
20	20	0.01/0.03
30	20	0.01/0.03

it can be shown that such large differences in residual strength can be explained entirely by the difference in the crack geometry. In these equations K_{IC} is the fracture toughness of the workpiece material, c the depth of the critical crack and f a geometric factor which can be set to 1 for very elongated cracks and to 0.63 for half-penny ones [39]. As in Equation 9, Θ is 90° or 0° for transverse (T) or longitudinal grinding (L), respectively. If the extreme values of f together with $c(T) > c(L)$ are used in Equation 10, the result is

$$\frac{\sigma_T}{\sigma_L} = 0.63 \left(\frac{c(L)}{c(T)}\right)^{1/2} < 0.63 \qquad (12)$$

which is close to the strength reduction reported above of 50%.

2.4. The residual strength of a ground component

If the assumption that the strength-limiting surface flaws after grinding with diamond tools are of the same kind as those caused by a Vicker's indenter it ought to be possible to replace the indenter load P in Equation 7 with the total grinding force P_{tot}. Since the latter depends on the machine parameters, a combination of Equations 7, 8, 9 and 11 will result in the equation

$$\sigma = \sigma_0 + \{\tfrac{256}{27}\,[\pi 1.25(1 - 0.37\cos\Theta)^2]^{3/2} B \times (\cot\Psi)^{2/3}\}^{-1/3} \left(\frac{H}{E}\right)^{1/6} K_{IC}^{4/3} P_{tot}^{-1/3}, \qquad (13)$$

TABLE II The properties of the diamond wheels used in this investigation

Diamond wheel	Bond type	Concentration	Grit size (mesh)
A	resin	50	400
B	metal	75	120
C	metal	50	320

with which it is possible to estimate the influence of the machine parameters on the residual strength. Here σ_0 is the residual stress existing in the surface prior to the last pass of the diamond wheel. If more than one pass is performed σ_0 ought to be the residual stress caused by the grinding. One can assume that σ_0 will be influenced by the machine parameters, but this dependence is difficult to postulate.

In Table I Equation 13 has been used to show schematically how the residual strength will depend on some grinding parameters.

3. Experiments

The workpiece material used in this investigation was hot isostatically pressed silicon nitride, manufactured by ASEA. It was delivered in three pieces, out of which test bars, 3.5 mm x 4.5 mm x 45 mm, were sawn. Since the pieces came from the same batch the material was probably homogeneous.

The grinding was performed on a surface grinder, Malcus 80. During grinding both the vertical and the horizontal forces were measured. Three different diamond wheels were used and their properties are given in Table II.

The machine parameters wheel speed, workpiece velocity and depth of cut were varied in such a way that each wheel was used for twelve different parameter combinations, given in Table III.

Longitudinal grinding was chosen since the total grinding force according to the proposed model is equal to the vertical force. Some additional test bars, however were transversely ground with wheel C. In the latter case the number of bars was limited and hence the depth of cut was set to 10 μm only.

The residual strength was measured in a four-point-bend with inner and outer spans of 20 mm and 40 mm, respectively. The beam rate was 0.5 $mm\,sec^{-1}$ and to prevent failures caused by

edge flaws, all the bars were manually chamfered prior to bending.

4. Results

4.1. Vertical grinding force

According to Equation 6 a straight line ought to have been the result when the vertical grinding force was plotted as a function of the machine parameters. However, this was not the case. Instead, two parallel lines were obtained, one for each depth of cut. The result indicates that Equation 6 should be modified in such a way that it will be able to describe cases where the machine parameters not are raised to the same powers, i.e.

$$P_v = P_{0v} + u_0 C_0 \left(\frac{v^x d^y}{V^z}\right) w, \qquad (14)$$

where x, y and z depend on the workpiece material and the construction of the diamond tool.

By setting $P_{0v} > 0$, iterative calculations for all wheels gave values close to 0.5, 1.0 and 0.5 for x, y and z, respectively. The results presented in Fig. 4 and Table IV show that when these values were used, a plot of the vertical grinding forces as a function of the machine parameters resulted in straight lines for all the wheels. Also in the transverse case only the vertical force was used in the plot, since the horizontal forces in all cases were negligible.

4.2. Residual strength after grinding

Equation 13 can be rewritten as

$$\sigma = \sigma_0 + \frac{M}{P_v^{1/3}}, \qquad (15)$$

where

$$M = \left\{\tfrac{256}{27}\left[\pi 1.25(1 - 0.37\cos\Theta)^2\right]^{3/2} B \times (\cot\Psi)^{2/3}\right\}^{-1/3} \left(\frac{H}{E}\right)^{1/6} K_{IC}^{4/3} \qquad (16)$$

which is a constant when the workpiece material, diamond wheel and the grinding direction are specified.

By combining Equations 14 and 15 one obtains the expression

$$\sigma = \sigma_0 + \frac{M}{\left[P_{0v} + u_0 C_0 \left(\frac{v^x d^y}{V^z}\right) w\right]^{1/3}} \qquad (17)$$

with which it is possible to estimate how the residual strength will depend on the machine parameters.

TABLE IV Estimated values of P_0 and $u_0 C_0$ when Equation 14 is applied to the results from grinding with wheels A, B and C. The values of x, y and z in Equation 14 are set to 0.5, 1.0 and 0.5, respectively

Wheel	$P_{0v} \times 10^6$ (MN)	$u_0 C_0$ (MN m^{-2})	R^*
A	12	8210	0.98
B	42	12921	0.96
C	56	9280	0.98
C (transverse)	55	4245	0.87

*R is the correlation coefficient for the plotted lines.

In Fig. 5 the residual strength as a function of the machine parameters used during the longitudinal grinding with wheel C, is presented. The values of x, y and z in Equation 17 are given in Section 4.1.

It seems as if the data points in Fig. 5 represent two straight lines, one for each depth of cut. Since each line represents just six parameter combinations and the difference in residual strength is small, one data point can dramatically alter the slope of the line. Such points have been excluded during the regression analysis in order to obtain reasonable results. The results obtained from grinding with wheels A and B are best represented

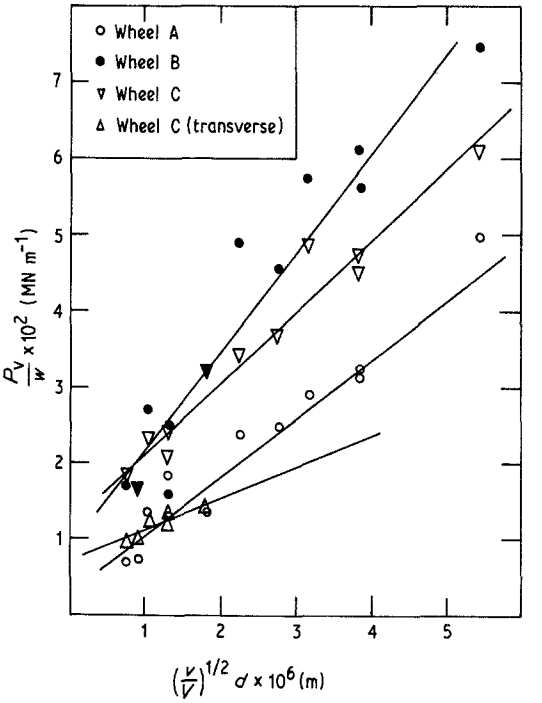

Figure 4 Normalized vertical grinding force, P_v/w, as a function of the machine parameters, according to Equation 14 and Table IV.

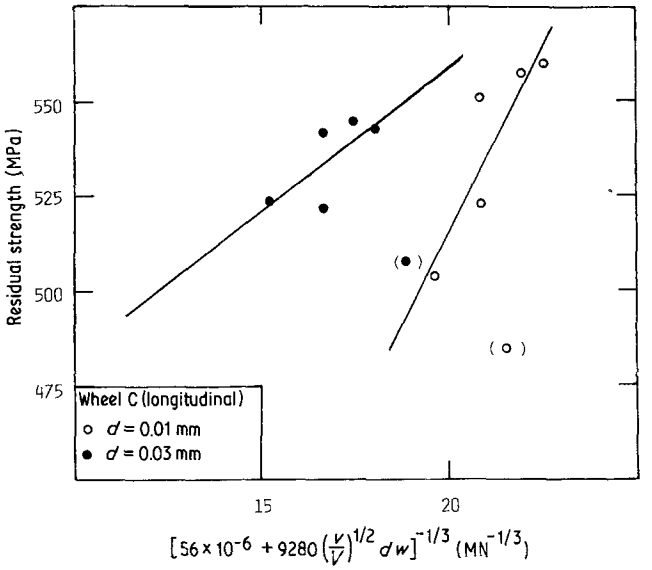

Figure 5 The residual strength as a function of the machine parameters, according to Equation 17. Data points within brackets have been excluded from the regression analysis.

by two separate lines, as can be seen from Fig. 6, in which the data from all grinding operations are presented schematically. The calculated values of σ_0 and M corresponding to the lines in Fig. 6 are given, in Table V.

4.3. Grinding defects

All fracture surfaces were examined in order to locate the fracture origins. With few exceptions, all fractures had originated from grinding defects.

According to Section 2.2 the surface cracks introduced during transverse and longitudinal grinding ought to be elongated and halfpenny-shaped, respectively. This was confirmed when some fracture surfaces of transversely (Fig. 7) and longitudinally (Fig. 8) ground test bars were examined in a scanning electron microscope (SEM).

The fracture surface of the test bar in Fig. 8 is especially interesting, since a number of half-penny cracks can be seen. All these cracks are located beneath grinding grooves. The largest crack, at which the fracture was initiated, is located beneath a very large grinding groove in the

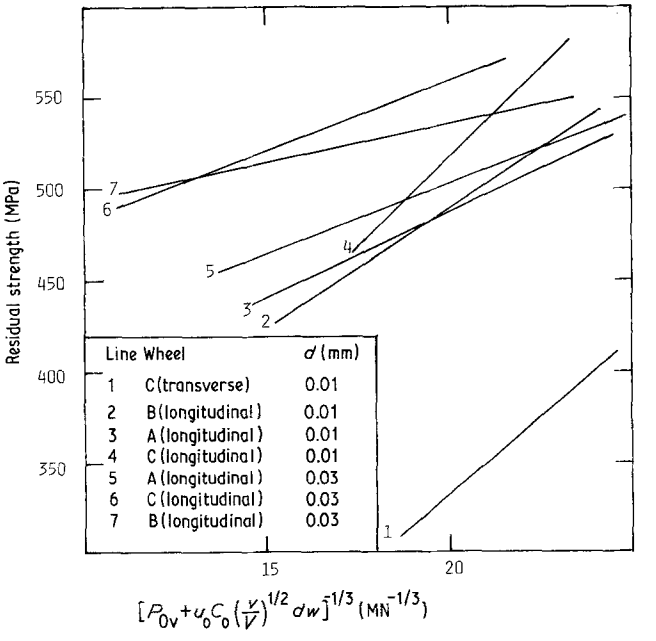

Figure 6 The residual strength as a function of the machine parameters, according to Equation 17. For all lines one or two data points have been excluded from the regression analysis.

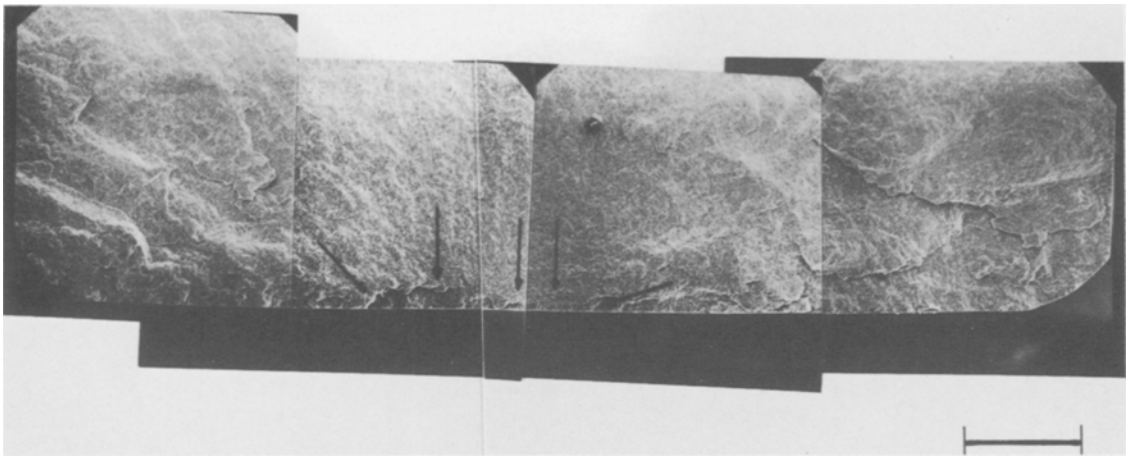

Figure 7 Fracture surface of a transversely ground test bar. The elongated surface crack is marked with arrows. Residual strength 377 MPa; crack depth 124 μm; $f = 0.94$. Bar = 500 μm.

lower right-hand corner of Fig. 8. In Fig. 9 this area is enlarged and a crack located orthogonally to the fracture surface, i.e. parallel to the grinding direction, can be seen. This means that two kinds of cracks are formed below each grinding groove, one elongated and a number of halfpenny ones, as is suggested in Fig. 3. It has been observed that the former cracks are deeper than the latter [9, 12, 16]; this is confirmed in this investigation since the depths of the cracks in Figs. 8 and 9 were estimated to be 91 and 137 μm, respectively.

5. Discussion

5.1. Vertical grinding force

The results presented in Fig. 4 seem to indicate that the relationship between the vertical grinding force and the machine parameters can be expressed with Equation 14. The factors P_{0v}, u_0C_0, x, y and z depend on the workpiece material, the type and condition of the diamond tool. In this investigation their values were estimated through iterative calculations based on the results from grinding with twelve different parameter combinations per wheel. This number was probably too small to give anything but a rough estimate of the values, especially since P_{0v} was not measured experimentally. Another factor that probably has influenced the results is that the wheels were not dressed prior to each change of the machine parameters.

From Fig. 4 it can be seen that grinding with both the metal-bonded wheels (B, C) results in higher forces compared to the resin-bonded wheel A, which is consistent with [36]. The grinding forces tend to increase with the number of diamonds in contact with the workpiece [34], i.e. increased diamond concentration [34] or tool wear [8, 32–34]. The higher grinding forces of wheel B compared to those of wheel C can probably be explained by the higher diamond concentration of the former.

The only difference between the longitudinal and the transverse grinding with wheel A was that

TABLE V Estimated values of σ_0 and M when Equation 17 is applied on the results from the grinding with wheels A, B and C. The values of P_{0v} and u_0C_0 are given in Table IV

Wheel	Depth of cut (mm)	σ_0 (MPa)	M (MPa MN$^{-1/3}$)	R*
A	0.01	300	9	0.70
	0.03	350	8	0.87
B	0.01	290	9	0.87
	0.03	450	4	0.94
C	0.01	125	20	0.89
	0.03	405	8	0.73
C (transverse)	0.01	−15	17	0.93

*R is the correlation coefficient for the plotted lines.

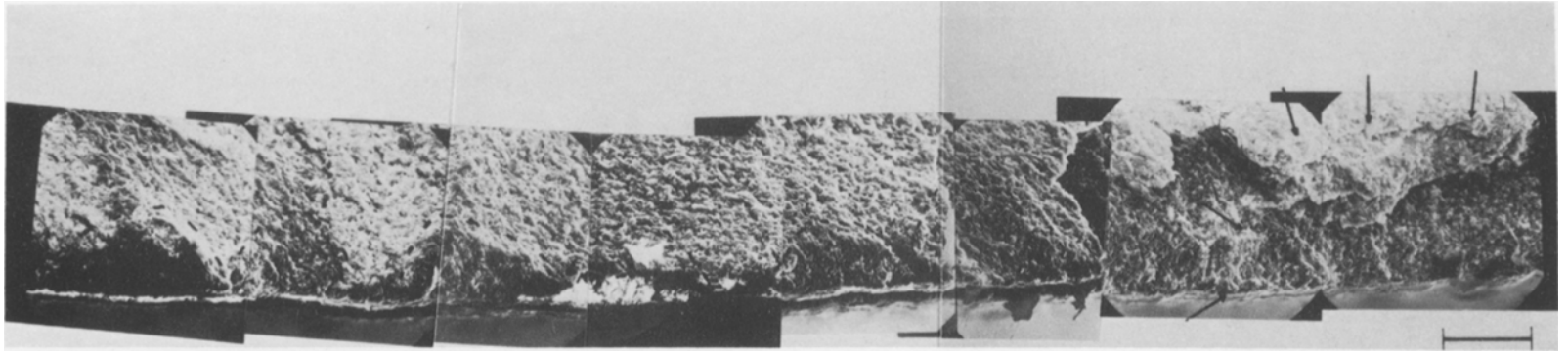

Figure 8 Fracture surface of a longitudinally ground test bar. The halfpenny-shaped crack which caused the failure is marked with arrows. Residual strength 492 MPa; crack depth 91 μm; $f = 0.66$. Bar = 50 μm.

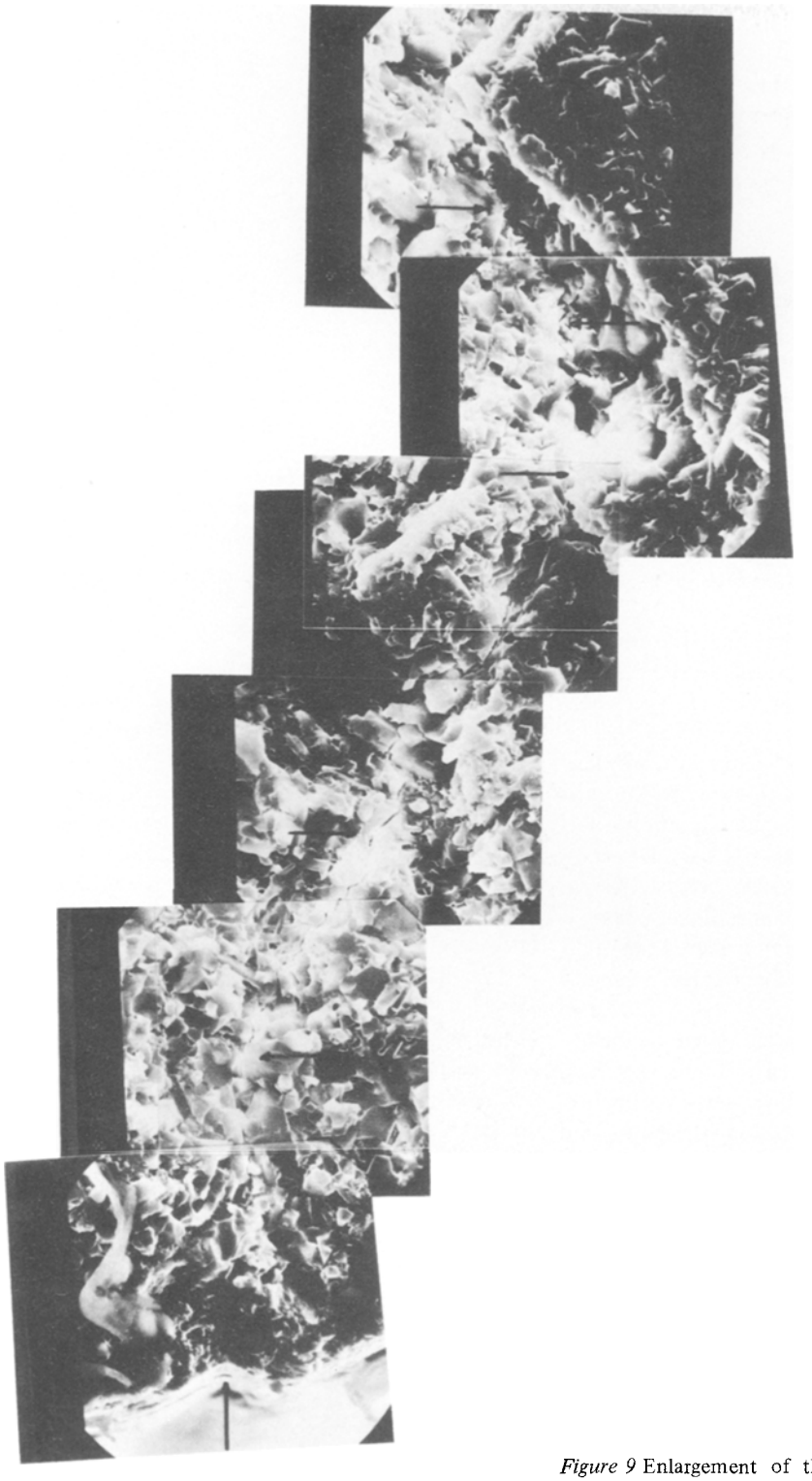

Figure 9 Enlargement of the area beneath the grinding groove which can be seen on the far right of Fig. 8. The crack is parallel to the grinding direction. The arrows mark the grinding groove and the crack. Crack depth 137 μm. Bar = 10 μm.

the grind width, w, was equal to the width of the test bars (4.5 mm) in the former case and to the wheel width (8 mm) in the latter. From Fig. 4 it can be seen that the vertical forces were of the same magnitude during grinding. The somewhat lower slope of the line representing the transverse grinding can probably be explained by the inaccuracy of the iterative calculation method.

5.2. Residual strength

Since the results presented in Fig. 6 agree fairly well with the predictions made in Table I, the proposed model seems to be feasible, i.e. the surface flaws caused by grinding are of the same kind as those caused by a Vicker's indenter. However, the influence of the depth of cut on the residual strength seems to be a bit strange, since the latter increases instead of decreases with an increased depth of cut. This result probably is an effect of the residual compressive stresses which have been introduced in the surface layer of the workpiece during the grinding.

In Table I it was predicted that the residual strength would be less influenced by the residual stress than by the depth of the surface flaws when the machine parameters were changed in such a way that the grinding forces were increased. The results in Fig. 6 indicate that this may be the case for the wheel speed and table velocity but not for the depth of cut. In the latter case the increase of the residual compressive stresses seems to be of such a magnitude that it overcomes the decrease in residual strength caused by the increased depth of the surface flaws, and thus the residual strength increases with the depth of cut.

In Fig. 6 it can be seen that although the metal-bonded wheels (B, C) resulted in higher grinding forces, the residual strength seems to be higher compared to when a resin-bonded wheel (A) was used. This probably means that the former wheels introduced higher residual stresses than the latter.

Fig. 6 also shows that the coarser wheel B results in lower residual strengths than the finer wheel C which is consistent with [5].

In this investigation the residual stresses were not measured experimentally, hence no attempt has been made to derive theoretically a relationship between the machine parameters, the material properties of the workpiece and the resulting residual stresses. One way to estimate the residual surface stresses would be to use the indentation technique and Equation 7. This is exemplified

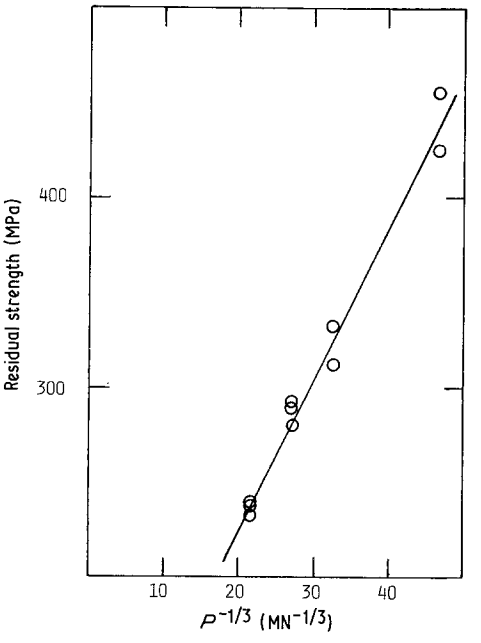

Figure 10 Residual strength of indented test bars as a function of the indenter load.

with Fig. 10 in which the residual strengths of indented test bars are plotted as a function of the used indenter loads. The compressive residual stress in this case was estimated to be 60 MPa.

The slope in Fig. 10 was calculated to 8 MPa $MN^{-1/3}$ which is of the same magnitude as those presented in Table V, and thus confirms that machining with diamond tools causes similar surface defects to those produced by an indenter.

The magnitude of the residual stresses given in Table V varies between −450 and +15 MPa. These values are of course incorrect since they have been estimated under the assumption that the residual stresses introduced during grinding do not depend on the machine parameters. If the fracture toughness of this material is set to 5.5 MPa $m^{1/2}$ and the values given for f and c in Figs. 7 and 8 are used in Equation 10 one obtains fracture strengths 264 and 443 MPa, respectively. The measured values, however, were 377 and 492 MPa, and thus the compressive stress level can be estimated as 113 and 49 MPa, respectively. Several similar calculations were made and they all showed that grinding had resulted in a compressive surface layer and that a reasonable magnitude of the stresses would be 65 to 150 MPa. This is consistent with reported compressive surface stresses, 135 to 170 MPa, in ground alumina [40].

5.3. Surface flaws

Examination of the fracture surfaces clearly showed that the failures were caused by grinding defects. It was confirmed that the flaws parallel to the grinding direction were deeper and more elongated than those perpendicular to it.

It was also observed that the longitudinally ground specimens often failed from corner cracks, which influence the residual strength. The transversely ground specimens, however, in all cases failed from surface cracks. It is thus recommended to use transverse grinding in future investigations, especially since most components will be used in such a way that the principal stress will not be parallel to the grinding direction.

In the model it is assumed that the elongated cracks parallel to the grinding direction are in principal as long as the grinding grooves, while the perpendicular ones are halfpenny shaped. However, in the latter case an elliptical crack can be formed if two or more halfpenny-shaped ones coincide. Such a crack is sketched in Fig. 3 (Section 2.3).

The geometric factor f is always rather close to 1 for elongated cracks while it varies quite considerably for those perpendicular to the grinding direction, depending on how many halfpenny cracks are interacting with each other. The lower limit is 0.63, one crack, but such extreme values as 0.91 have been measured in this investigation. The variation in f probably explains why the Weibull modulus shows a tendency to be higher for transversely ground bars than for longitudinally ground bars. This was the case in this investigation and such tendencies can also be found in the literature [5, 9].

6. Conclusions

This investigation presents a model in which it is assumed that the mechanisms which cause cracks beneath both an indenter and a diamond tool are the same. Hence it ought to be possible to combine already established equations from these two fields to form an expression with which it is possible to estimate how the choice of machining parameters will influence the residual strength.

The experimental results show that the proposed model is feasible and that:

1. grinding with diamond tools introduces cracks and residual compressive stresses in the surface layer of the workpiece;

2. the cracks parallel to the grinding direction are more elongated and deeper than those perpendicular to it, hence longitudinal grinding results in higher residual strengths than transverse grinding;

3. the depth of the cracks and the magnitude of the residual stresses depend on the grinding forces;

4. the grinding forces increase with the workpiece velocity and the depth of cut, respectively, and decrease with an increased wheel speed;

5. the use of coarser diamond wheels results in a lower residual strength;

6. compared to resin-bonded wheels, metal-bonded ones result in higher grinding forces, residual stresses and residual strengths.

Acknowledgements

The grinding was performed at the Department of Production Engineering, Royal Institute of Technology in Stockholm, and the author thanks the head of this department, Professor Bo Lindström, for helpful discussions. The work was partly sponsored by the National Swedish Board for Technical Development under contract 81-3508.

References

1. H. E. HELMS and J. A. BYRD, ASME 82-GT-253.
2. R. N. KATZ and E. M. LENOE, in Proceedings of the Automative Development Contractors Meeeting, 26–29 October, 1981, Dearborn, Michigan (National Technical Information Service, US Department of Commerce, Springfield, VA) p. 511.
3. T. YOSHIMITSU *et al.*, SAE 820431.
4. R. KAMO, in Proceedings of the Fifth Army Materials Technology Conference, Newport, Rhode Island, 21–25 March 1977, edited by J. J. Burke, E. N. Lenoe and R. N. Katz (Brook Hill Publishing Co., Chesnut Hill, MA, 1978) p. 907.
5. C. A. ANDERSSON, R. J. BRATTON, S. C. SANDAY and A. COHN, *ibid.* p. 783.
6. D. W. RICHERSON, J. J. SCHULDIES, T. M. YONUSHONIS and K. M. JOHANSEN, *ibid.*, p. 625.
7. C. CM. WU and K. R. MCKINNEY, in "The Science of Ceramic Machining and Surface Finishing II", edited by B. J. Hockey and R. W. Rice, National Bureau of Standards Special Publication 562 (US Government Printing Office, Washington, DC, 1979) p. 477.
8. H. P. KIRCHNER, R. M. GRUVER and D. M. RICHARD, *ibid.*, p. 23.
9. C. A. ANDERSSON and R. J. BRATTON, *ibid.*, p. 463.
10. T. E. EASLER, T. A. COUNTERMINE, R. E. TRESSLER and R. C. BRADT, *ibid.*, p. 455.
11. A. MALKING and M. HUERTA, *ibid.*, p. 93.
12. R. W. RICE and J. J. MECHOLSKY JR., *ibid.*, p. 351.
13. R. W. RICE, *ibid.*, p. 429.

14. R. W. RICE and B. K. SPERONELLO, *J. Amer. Ceram. Soc.* **59** (1976) 330.
15. R. W. RICE, in Proceedings of the Second Army Materials Technology Conference Hyannis, Massachusetts, 13–16 November 1973, edited by J. J. Burke, A. E. Gorum and R. N. Katz (Brook Hill Publishing Co., Chestnut Hill, MA, 1974) p. 287.
16. R. W. RICE, J. J. MECHOLSKY JR and P. F. BECHER, *J. Mater. Sci.* **16** (1981) 853.
17. R. W. RICE, in "The Science of Ceramic Machining and Surface Finishing I", edited by S. J. Schneider and R. W. Rice, National Bureau of Standards Special Publication 348 (US Government Printing Office, Washington DC, 1972) p. 365.
18. R. SEDLACEK, F. A. HALDEN and P. J. JORGENSEN, *ibid.*, p. 391.
19. *Idem, ibid.*, p. 89.
20. H. KESSEL and E. GUGEL, *Industrie Diamanten Rundschau* **11** (1977) 3.
21. K. HECKEL and H. HEIGEL, *ICM 3* **3** (1979) August p. 27.
22. E. RABINOWICZ, *Wear* **39** (1976) 101.
23. M. V. SWAIN, *Proc. Roy. Soc. Lond. A* **366** (1979) 575.
24. D. B. MARSHALL, in "Progress in Nitrogen Ceramics", edited by F. L. Riley, NATO ASI Series E (Martinus Nijhoff Publishers, Haag, 1983) p. 635.
25. H. R. BAUMGARTNER and P. E. COWLEY, Final Report, Contract DAAG46-74-C-0055, National Technical Information Service (US Department of Commerce, Springfield, VA, 1976).
26. B. R. LAWN, A. G. EVANS and D. B. MARSHALL, *J. Amer. Ceram. Soc.* **63** (1980) 574.
27. P. CHANTICUL, G. R. ANSTIS, B. R. LAWN and D. B. MARSHALL, *ibid.* **64** (1981) 539.
28. B. RINGVALL, in "Slip Naxos Handbok i Slipning, Karleboserien 19 Maskinbolaget Karlebo i samarbete med aktiebolaget" (Slipmaterial Naxos, Stockholm, 1972).
29. B. COLDING, Slipprocessen – Teori, Kompendium (Royal Institute of Technology, Stockholm, 1970).
30. B. G. KOEPKE and R. J. STOKES, in "The Science of Ceramic Machining and Surface Finishing II", edited by B. J. Hockey and R. W. Rice, National Bureau of Standards Special Publication 562 (US Government Printing Office, Washington DC, 1979) p. 75.
31. P. J. GIELISSE, T. J. KIM and A. CHOUDRY, *Mater. Sci. Res.* 7 (1974) 137.
32. I. IDA, Y. ARAI and K. INAMORI, *Ann. CIRP* **17** (1969) 259.
33. I. IDA, Y. ARAI, M. FUKUDA, K. INAMORI and M. SUGIURA, *Rev. Electr. Com. Lab.* **17** (1969) 1056.
34. Y. UENO, Y. ARAI, I. IDA and M. FUKUDA, *ibid.* **18** (1970) 141.
35. T. J. KIM and P. J. GIELISSE, *Int. J. Prod. Res.* **17** (1979) 155.
36. H. O. JUCHEM and H. WAPLER, *Ind. Diamond Rev.* Feb (1979) p. 43.
37. W. WEILAND, *Keramische Zeitschrift* **28** (1976) 645.
38. G. R. ANSTIS, P. CHANTIKUL, B. R. LAWN and D. B. MARSHALL, *J. Amer. Ceram. Soc.* **64** (1981) 533.
39. J. CARLSSON, Brottmekanik, Ingenjörsförlaget AB, Stockholm (1976).
40. F. F. LANGE, M. R. JAMES and D. J. GREEN, *J. Amer. Ceram. Soc.* **66** (1983) C-16.

Received 2 April
and accepted 10 May 1984